Thermochimica Acta 519 (2011) 83–89

Contents lists available at ScienceDirect

Thermochimica Acta

journal homepage: www.elsevier.com/locate/tca

Kinetics and mechanism of structural transformations of $Fe_{75}Ni_2Si_8B_{13}C_2$ amorphous alloy induced by thermal treatment

D.G. Minić[c], V.A. Blagojević[a], Lj.E. Mihajlović[a], V.R. Ćosović[b], D.M. Minić[a,*]

[a] Faculty of Physical Chemistry, University of Belgrade, 11000 Belgrade, Serbia
[b] Technology and Metallurgy, Department of Materials and Metallurgy, University of Belgrade, 11000 Belgrade, Serbia
[c] Kontrola LLC, Austin, TX, United States

ARTICLE INFO

Article history:
Received 10 January 2011
Received in revised form 14 February 2011
Accepted 26 February 2011
Available online 21 March 2011

Keywords:
Amorphous materials
Metallic glasses
Metals and alloys
Thermal analysis
Phase transition

ABSTRACT

The kinetics of structural transformations of the $Fe_{75}Ni_2Si_8B_{13}C_2$ amorphous alloy under non-isothermal conditions was studied. It was shown that the amorphous alloy was stable up to 723 K, when multi-step structural transformations start, involving formation of stable α-Fe(Si) and Fe_2B crystalline phases, and a metastable $Fe_{15}Si_3B_2$ phase, their growth and the decomposition of the metastable phase into the two stable phases. Peakfit software was used to resolve the overlapping peaks corresponding to different crystallization steps, at different heating rates. The kinetic parameters corresponding to each of the steps were evaluated and kinetic triplet for every single step was established ($g(\alpha) = [-\ln(1-\alpha)]^{1/3}$, $E_a = 375.1 \pm 0.8$ kJ/mol and $\ln A = 56.2 \pm 1.0$ for step 1; $E_a = 341.6 \pm 0.5$ kJ/mol and $\ln A = 49.3 \pm 0.5$ for step 2). The effects of structural transformations on the established kinetic model were discussed in detail.

1. Introduction

Metallic glasses are kinetically and thermodynamically metastable materials. They are usually stable at room temperature and transform to more stable crystal forms at higher temperatures [1]. Due to their excellent soft magnetic properties, such as high saturation magnetization, high permeability, low coercivity and loss, these materials are used in many different applications, such as power devices, information technology, magnetic sensors, anti-theft security systems [2,3]. The change in structure can lead to change in their technologically important properties, such as the heat capacity, electrical resistivity, volume and magnetic properties [4–7]. This can, sometimes, improve their performance, but it can also deteriorate it, making them suitable for single-use only. This makes it important to study kinetics of phase transformations induced by thermal treatment of amorphous alloys.

Our research of Fe-based amorphous alloys showed that, at high temperatures, thermally treated amorphous alloys undergo single- or multi-step processes of structural phase transformations. The kinetics of these processes was investigated in detail [8,9]. We also studied the structural transformations of the $Fe_{75}Ni_2Si_8B_{13}C_2$ amorphous alloy under non-isothermal as well as under isothermal conditions [10]. These studies showed that the $Fe_{75}Ni_2Si_8B_{13}C_2$ amorphous alloy was stable up to the temperature of 723 K when multi-step structural transformations began. The primary crystallization already started at 723 K with formation of α-Fe(Si) phase in the amorphous matrix. At higher temperatures (between 780 and 800 K) we detected the presence of the boron–iron–silicon phase ($B_2Fe_{15}Si_3$) as well as the iron–boron (Fe_2B) phase. Above 870 K only two phases, Fe_3Si and Fe_2B, were detected. The present paper is concerned with the study the non-isothermal mechanism and kinetics of multi-step processes of structural transformations of $Fe_{75}Ni_2Si_8B_{13}C_2$ amorphous alloy in 293–1273 K temperature range, with particular emphasis on correlation of structural transformations and the kinetic parameters.

2. Experimental procedure

2.1. Materials and techniques

The ribbon-shaped samples of $Fe_{75}Ni_2Si_8B_{13}C_2$ amorphous alloy (2 cm wide and 35 μm thick) were obtained using the standard procedure of rapid quenching of the melt on a rotating disc (melt-spinning method).

The thermal stability of the alloy as well as its structural transformations have been investigated by the differential scanning calorimetry (DSC) in a nitrogen atmosphere using a DSC-50 analyzer (Shimadzu, Japan). In this case, samples weighing several milligrams were heated in the DSC cell from room temperature

* Corresponding author. Tel.: +381 11 3336 689.
E-mail addresses: dminic@ffh.bg.ac.rs, drminic@gmail.com (D.M. Minić).

0040-6031/$ – see front matter © 2011 Elsevier B.V. All rights reserved.
doi:10.1016/j.tca.2011.02.040

to 973 K in a stream of nitrogen with a flow rate of 20 ml min^{-1} at different heating rates. The overlapping exo-peak was resolved using *Peakfit* software version 4.11 [11,12]. The peak resolution was conducted using a combination of Gaussian and Lorentzian functions. Only the fitted peaks with correlation factor $R^2 > 0.995$ were accepted as a good fit.

2.2. Solid-state kinetic analysis

All kinetic analyses of solid-state transformations are based on a single-step kinetic equation:

$$\frac{d\alpha}{dt} = k(T)f(\alpha) \quad (1)$$

where $k(T)$ is the rate constant, t is the time, T is the temperature, α is the fractional extent of reaction (rate conversion), and $f(\alpha)$ is a conversion function (kinetic model) which depends on the particular reaction model.

The temperature dependence of the rate conversion is introduced by replacing $k(T)$ with the Arrhenius equation, which gives the relation:

$$\frac{d\alpha}{dt} = A\exp\left(-\frac{E}{RT}\right)f(\alpha) \quad (2)$$

where A (pre-exponential factor) and E (activation energy) are the Arrhenius parameters and R is the gas constant.

Kinetic description of solid state transformations usually includes a kinetic triplet, involving Arrhenius parameters (activation energy, E and pre-exponential factor, A) as well as an algebraic expression of the conversion function, $f(\alpha)$ describing the dependence of the reaction rate on the conversion degree, α.

In solid state reactions, the constant value of activation energy can be expected only for a single-step reaction and E in Eq. (2) becomes an apparent quantity (E_a), based on a quasi-single-step reaction. In non-isothermal measurements at constant heating rate, β, Eq. (2) transforms to:

$$\beta\frac{d\alpha}{dT} = A\ \exp\left(-\frac{E_a}{RT}\right)f(\alpha) \quad (3)$$

where $d\alpha/dt \equiv \beta(d\alpha/dT)$.

The rate conversion $d\alpha/dt$ is proportional to the measured specific heat flow Φ, normalized per sample mass (W g^{-1}):

$$\frac{d\alpha}{dt} = \frac{\phi}{\Delta H} \quad (4)$$

where ΔH corresponds to the total enthalpy change associated with the solid-state transformations. The fractional extent of reaction α can easily be obtained by partial integration of non-isothermal thermal analysis curve.

3. Results and discussion

3.1. Thermal behavior and structural transformations induced by thermal treatment

As-prepared $Fe_{75}Ni_2Si_8B_{13}C_2$ alloy is stable up to a temperature of 723 K when the multi-step crystallization begins, exhibiting overlapping crystallization peaks in DSC (Fig. 1), between 790 and 900 K, depending on the heating rate [10].

The appearance of such overlapping peaks in the process of crystallization of amorphous alloys could be provoked by several stages of crystallization of compounds involving different constituents, produced during a reaction, or by crystallization of compounds involving same constituents in several different stoichiometries. The overlapping peaks can also indicate that the nucleation and growth of crystals take place simultaneously. In overlapping peaks, there are intervals where the experimental data corresponds only to the summed values of multiple individual steps, rather than to any individual step in particular. If the overlap is negligible (the second step begins as first one is almost finished) this can be ignored, but when the degree of overlap is significant (in simultaneous steps) it is necessary to resolve the complex peaks.

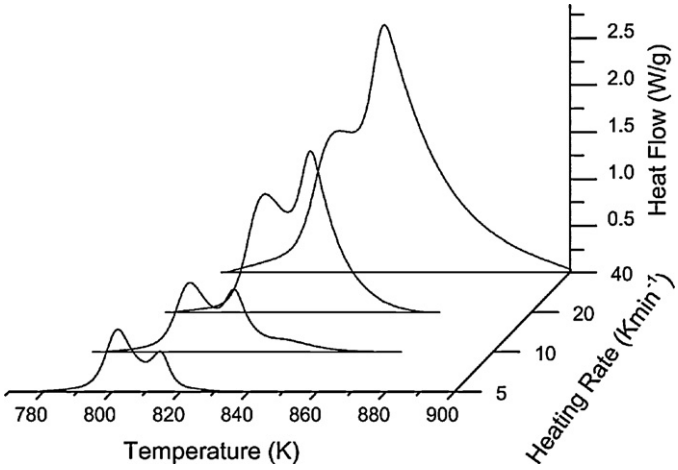

Fig. 1. DSC curves of alloy at different heating rates.

The resolution of the complex peaks yielded two well separated peaks for heating rate 5 K min^{-1} and three for the higher heating rates (Fig. 2).

Fig. 2a and b shows the experimental (dashed lines) and resolved DSC curves (solid lines) at heating rates 5 and 10 K min^{-1}, respectively. The changes in intensities and characteristic temperatures with the heating rate indicate that the heating rate has a significant influence on the crystallization process. As the heating rate is increased, the intensities of all DSC peaks increase and they shift to higher temperatures, indicating thermal activation of the observed steps of the crystallization process. The ratios of peak intensities and the intervals between the peaks change with the increasing heating rate, as the activation energies of individual crystallization steps are different.

The overall activation energy of different crystallization steps, as well as the pre-exponential factors under linear heating conditions were determined by the Kissinger's, as well as the Ozawa's peak methods, based on the dependence of exothermic peak temperature T_p on heating rate β [13,14], Table 1. When compared to our previous study of this system, conducted using Kissinger's and Ozawa's methods on unresolved peaks [10], the values obtained for resolved peaks are slightly lower, but they are within the range of experimental error of those data. The resolution of peaks, however, resulted in much lower experimental error, when compared to analysis of unresolved peaks.

The high values of the apparent activation energy of crystallization of amorphous alloy indicate primarily the high complexity of these processes, as well as the fact that a lot of atoms are involved in an elementary step of structural reorganization. The errors were determined as a root-square deviation multiplied on Student's coefficient for the probability of 0.95.

3.2. Determination of kinetic triplets

In order to establish kinetic description of the crystallization process, we applied "the model free", as well as "the model fitting" method. The fraction extent of reaction, α, at any temperature, T, for all crystallization steps was obtained as $\alpha = S_T/S$, where S is the total area of the exothermal curve between the temperature T_i, where the crystallization is just beginning, and the temperature T_f, where the crystallization is completed. S_T is the area between the initial

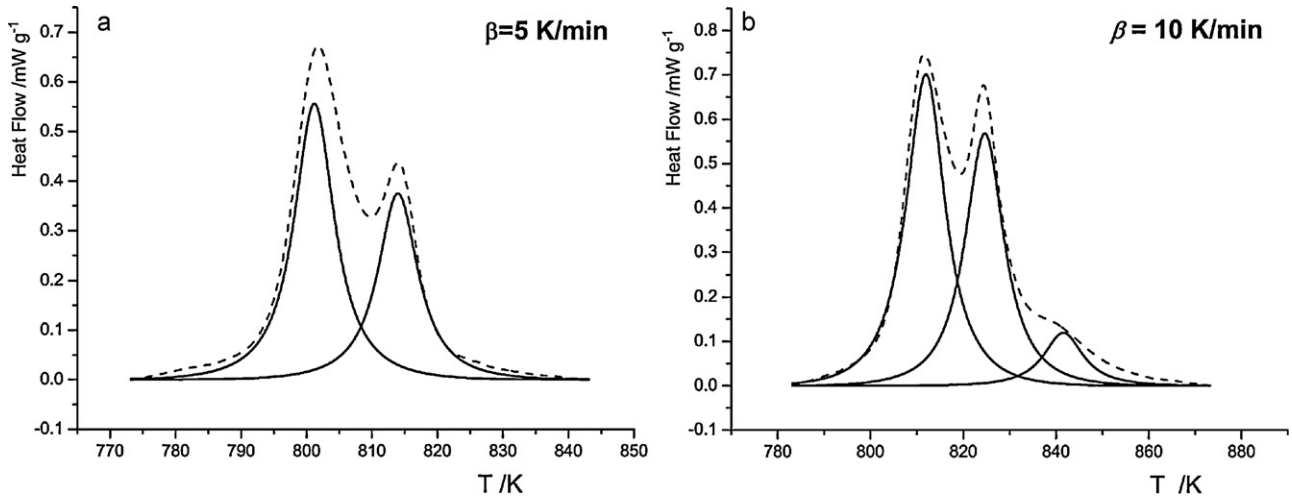

Fig. 2. The resolved DSC peaks for heating rates (a) 5 K min^{-1} and (b) 10 K min^{-1}.

temperature and a generic temperature, T, ranging between T_i and T_f.

3.2.1. Model free approach

The model-free approach, also known as "isoconversion method", requires determination of the temperature T_α at which an equivalent stage of the reaction occurs for various heating rates. The widely accepted procedure, giving the influence of fractional extent of reaction, α, on the values of kinetic parameters, is the Flynn–Wall–Ozawa's (FWO) method [15,16] in the form:

$$\ln\ \beta = \ln\left(\frac{AE_{a,\alpha}}{Rg(\alpha)}\right) - 1.0518\frac{E_{a,\alpha}}{RT_\alpha} \tag{5}$$

where $g(\alpha)$ is the integral form of the conversion function $f(\alpha)$, and defined as $g(\alpha) = \int (d\alpha)/(f(\alpha))$.

In accordance with Eq. (5), the dependence of $\ln\beta$ on $1/T$ allows us to determine apparent activation energy, even without the knowledge of the correct conversion function. The values of the apparent activation energies, calculated from the slope of this dependence, and intercepts, are shown in Fig. 3 as a function of the conversion degree. It can be observed that, for the first two crystallization steps, the determined apparent activation energies, as well as intercepts of obtained dependences, are practically constant in α range of 0.3–0.8 indicating a single step processes. The continuous decrease in the dependences of the third step indicates a complex process, which could not be considered as a single step [17]. Accordingly, it is not possible to determine the unique kinetic triplet for this step. The same shape of obtained dependences suggests that the apparent activation energy as well as the intercepts depend in the same way on the fraction extent of the considered processes.

3.2.2. Model fitting approach

Taking into account that the first two crystallization steps can be treated as single step processes, we used model fitting method, applying the Coats–Redfern method [18] for different forms of conversion functions for solid state reactions, to determine the kinetic triplets for the first two crystallization steps. The criterion for choosing the right conversion function was the linearity correlation factor, R^2, of dependence $f(\alpha) = f(1/T)$ at different heating rates for individual steps, Table 2.

Although all correlation coefficients R^2 (Table 2) are very close to 1, the Arrhenius parameters for applied heating rates are highly variable, exhibiting strong dependence on the selected conversion function. This means that, under non-isothermal conditions, $\alpha = f(T)$ curves and Coats–Redfern's method do not permit us to determine the true kinetic parameters as well as the correct conversion function. This is due to the fact that kinetic curves contain information about the temperature and conversion components in non-separate form. In order to find the true conversion functions for first and second step of crystallization, we have chosen the values of apparent activation energies determined using Kissinger's method and applied some additional criteria, such as the independence of the activation parameters on the heating rate [19], master plot method [20] and analysis of two new functions defined by Málek [21–23].

In order to determine which of the conversion functions presented in Table 2 best corresponds to the first and the second crystallization step, we first applied the criterion of the independence of activation parameters on the heating rates on the conversion functions. According to this criterion [19], for the correct proposed conversion function, the following should be true:

$$\ln\left(\frac{\beta g(\alpha)}{T^2}\right) = \ln\left(\frac{AR}{E_a}\right) - \frac{E_a}{RT} \tag{6}$$

where $g(\alpha)$ is the integral form of kinetic model, defined as:

$$g(\alpha) = \int_0^\alpha \frac{d\alpha}{f(\alpha)} = \frac{ZE_a}{R\beta}p(x); p(x) = \int_0^x \frac{\exp(-x)}{x^2}dx; x = \frac{E_a}{RT}$$

Using Eq. (6) for different conversion functions, Table 2, we tested the applicability of the criterion of the independence of acti-

Table 1
Kinetic parameters for the three crystallization steps determined by Kissinger and Ozawa methods.

Overall values	Step 1		Step 2		Step 3	
	Kissinger	Ozawa	Kissinger	Ozawa	Kissinger	Ozawa
E_a [kJ mol^{-1}]	375.1 ± 0.8	388.7 ± 0.8	341.6 ± 0.5	355.4 ± 0.5	330 ± 10	344.7 ± 10
ln A	56.2 ± 1.0	49.1 ± 0.1	49.3 ± 0.5	43.4 ± 0.5	47 ± 12	41 ± 12
R	0.999	0.999	0.999	0.999	0.972	0.974

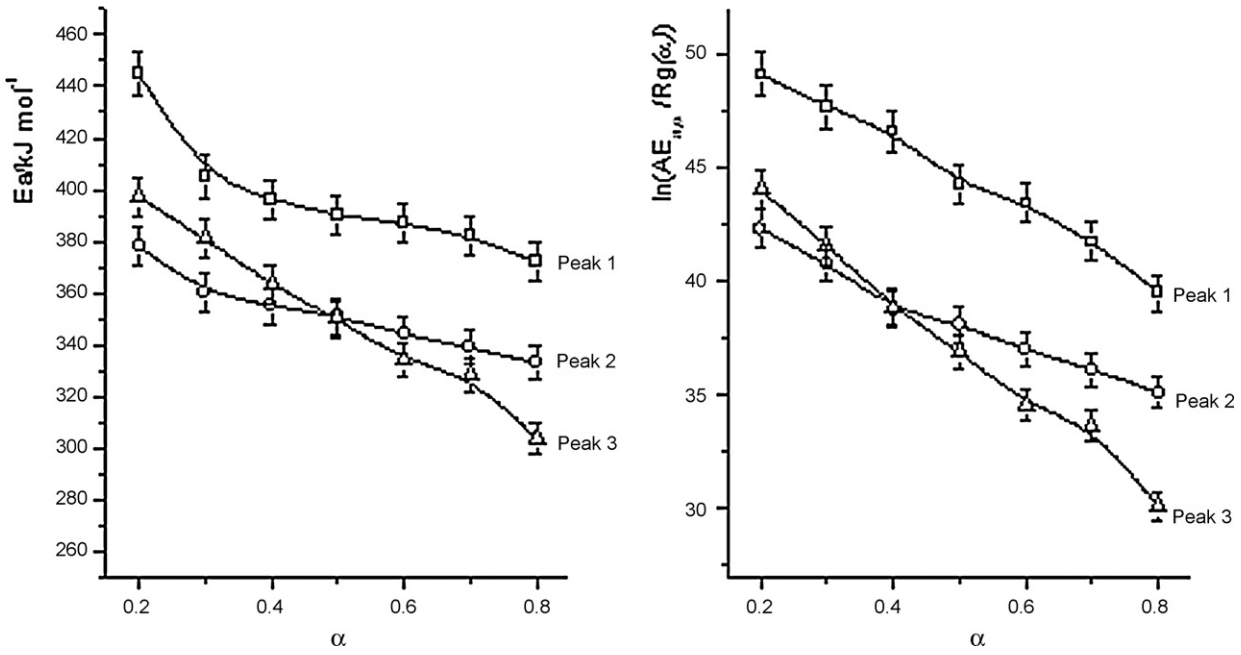

Fig. 3. Dependence of apparent activation energies E_a (a) and intercepts (b) on the conversion degree for different crystallization steps.

vation parameters on the heating rate. As a result, Fig. 4c, we obtained satisfactory linearity only for JMA model in the form $g(\alpha)=[-\ln(1-\alpha)]^{1/n}$ where $n=3$ for both steps of crystallization occurring as single-step processes is the most satisfactory.

Further verification of the applicability of this conversion function was conducted using Málek's [21–23] and master plot [20] methods. In order to apply Malek's method, we tested our experimental data using two special functions, $y(\alpha)$ and $z(\alpha)$. For JMA model, $y(\alpha)$ and $z(\alpha)$ functions have a convex shape, the maximum values being designated as α_y^* and α_z^*, respectively. For practical reasons these functions are usually normalized within [0,1] range. In non-isothermal conditions, these functions are

Table 2
Apparent parameters obtained by using the Coats–Redfern equation for different kinetic models at different heating rates.

Conversion function J		$\beta=5\,^\circ$C min^{-1}			$\beta=10\,^\circ$C min^{-1}			$\beta=20\,^\circ$C min^{-1}			$\beta=40\,^\circ$C min^{-1}		
		$\ln A$ (min^{-1})	E_a (kJ mol^{-1})	R^2	$\ln A$ (min^{-1})	E_a (kJ mol^{-1})	R^2	$\ln A$ (min^{-1})	E_a (kJ mol^{-1})	R^2	$\ln A$ (min^{-1})	E_a (kJ mol^{-1})	R^2
Peak 1	P4	37.5	261.2	0.984	33.4	233.2	0.986	33.9	234.5	0.981	21.3	148.9	0.982
	P3	50.9	349.1	0.984	45.4	312.1	0.986	45.7	313.9	0.982	29.1	201.0	0.983
	P2	76.9	535.8	0.985	69.8	479.9	0.987	70.7	482.7	0.982	45.4	311.6	0.984
	A3/2	128.2	859.0	0.994	112.8	761.9	0.990	114.6	778.8	0.991	72.0	492.1	0.987
	A2	96.3	647.5	0.991	84.8	573.9	0.990	86.3	586.7	0.991	54.1	369.4	0.987
	A3	62.9	426.8	0.991	55.4	377.7	0.990	56.6	386.1	0.991	35.2	241.4	0.986
	A4	46.2	317.1	0.990	40.7	280.2	0.990	41.8	286.5	0.991	25.8	177.8	0.986
	R1	161.9	1085.0	0.985	143.9	973.3	0.987	143.6	979.0	0.983	92.8	637.1	0.984
	R2	185.1	1242.6	0.985	164.4	1114.1	0.994	164.2	1122.2	0.991	105.9	730.2	0.992
	R3	193.7	1301.7	0.993	171.9	1166.9	0.996	171.7	1176.0	0.993	110.6	765.1	0.994
	D1	326.5	2183.4	0.985	290.0	1960.2	0.987	288.7	1971.7	0.983	186.8	1288.1	0.985
	D2	355.5	2379.3	0.990	315.6	2135.2	0.992	314.4	2149.7	0.988	203.2	1403.8	0.990
	D3	389.6	2614.6	0.995	345.5	2345.3	0.996	344.5	2363.7	0.993	222.1	1542.9	0.994
	D4	348.7	2343.2	0.993	306.9	2101.9	0.994	308.3	2117.9	0.992	198.6	1381.9	0.992
	F1	195.9	1308.4	0.995	172.3	1161.3	0.990	174.6	1187.0	0.991	122.5	837.8	0.987
Peak 2	P4	39.1	275.6	0.979	32.1	227.8	0.980	33.6	236.8	0.982	22.3	158.4	0.987
	P3	53.0	368.1	0.980	43.6	305.0	0.981	45.4	317.0	0.983	30.4	213.6	0.988
	P2	82.4	564.8	0.980	67.8	469.3	0.982	70.2	487.5	0.983	47.3	330.9	0.988
	A3/2	132.3	899.2	0.989	109.2	749.0	0.989	114.2	789.7	0.992	76.0	529.2	0.991
	A2	99.4	678.0	0.989	82.0	564.1	0.989	86.0	594.8	0.992	57.1	397.4	0.991
	A3	65.0	447.0	0.988	53.5	371.1	0.989	56.4	391.5	0.992	37.2	260.0	0.990
	A4	47.7	332.2	0.988	39.3	275.2	0.988	41.6	290.4	0.991	27.3	191.7	0.990
	R1	168.1	1143.1	0.981	138.6	952.3	0.982	142.6	988.8	0.984	96.6	676.0	0.989
	R2	192.5	1310.6	0.990	158.5	1091.5	0.990	163.0	1133.3	0.992	110.1	773.8	0.995
	R3	201.5	1373.5	0.992	165.8	1143.8	0.993	170.5	1187.4	0.994	115.0	810.5	0.996
	D1	339.0	2299.8	0.981	279.4	1918.3	0.982	286.7	1991.6	0.984	194.4	1366.0	0.989
	D2	369.4	2507.9	0.987	304.2	2091.3	0.988	312.2	2171.2	0.989	211.3	1487.7	0.993
	D3	405.2	2758.3	0.992	333.4	2299.4	0.993	342.0	2386.8	0.994	230.9	1633.7	0.997
	D4	362.6	2471.2	0.990	298.3	2059.9	0.991	306.2	2139.0	0.994	206.6	1463.8	0.995
	F1	202.1	1369.5	0.989	166.8	1142.0	0.989	174.0	1203.6	0.992	116.0	809.0	0.991

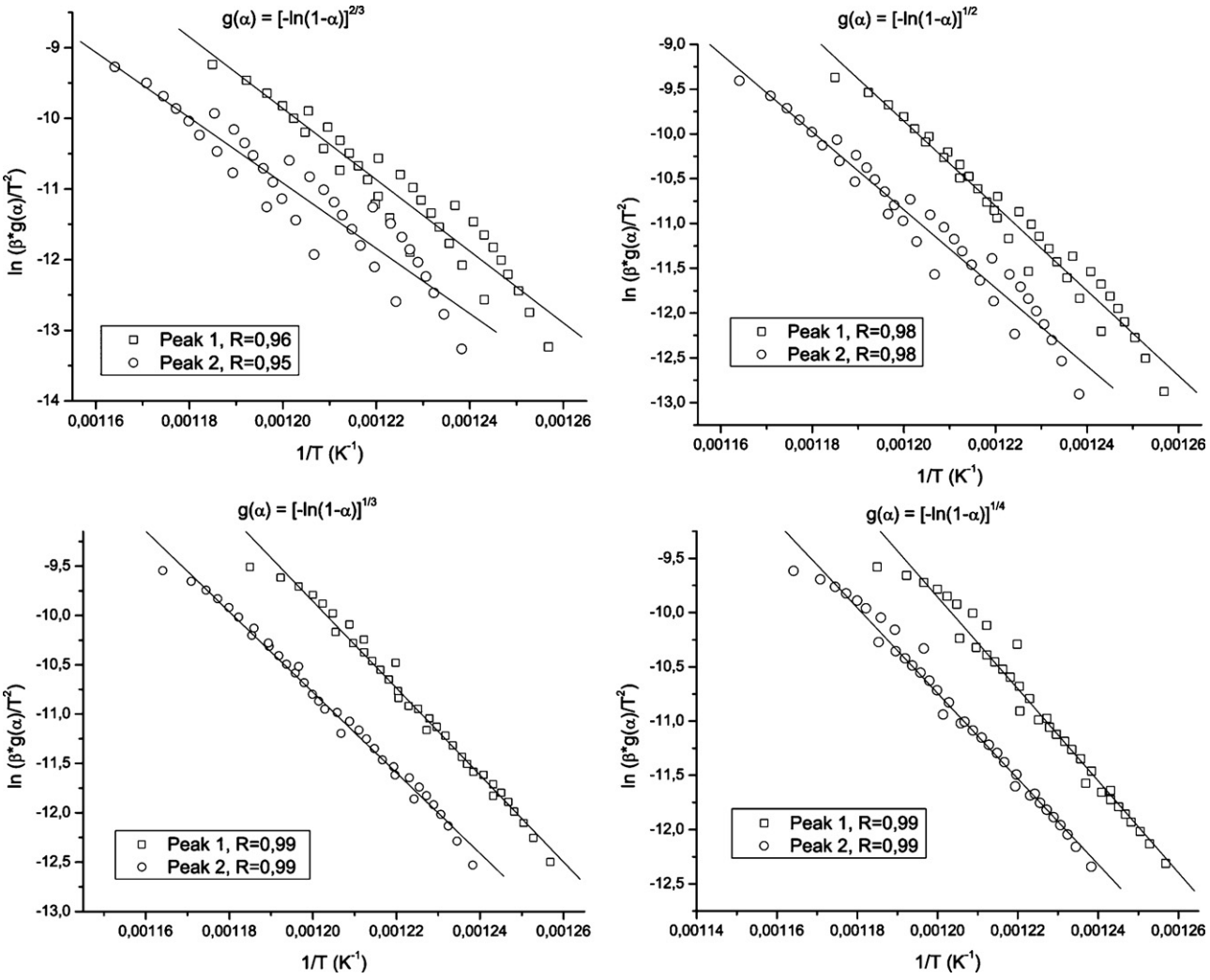

Fig. 4. Independence of activation parameters on the heating rates for different forms of JMA model, for the first and second crystallization peak.

defined as follows:

$$y(\alpha) = \left(\frac{d\alpha}{dt}\right) \exp\left(\frac{E_a}{RT}\right) = Af(\alpha) \tag{7}$$

$$z(\alpha) \approx \left(\frac{d\alpha}{dt}\right) T^2 \tag{8}$$

The "fingerprint" of JMA model is that the value of $\alpha_z^* = 0.632$ and that the value of α_y^* is always lower than the value of α_z^*, under the assumption that the crystal growth occurs only after the nucleation has been finished.

The convex shape of the obtained normalized functions $y(\alpha)$ and $z(\alpha)$ (Fig. 5), and their independence on the heating rate β, show that the proposed conversion function is correct for both crystallization peaks. Both functions exhibit well defined maxima located at an exactly defined values of α. However, the values of α_z^* are not 0.632, but 0.5, and the values of α_y^* are higher, at 0.6, instead of lower than the values of α_z^*. As JMA model [24,25] can be applied to non-isothermal conditions only under the assumption that the nucleation is completed before the further crystalline growth, the deviation from the model exhibited in our system indicates that this condition is not met. However, the correct shape of the curves indicates that JMA model approximates the reaction mechanism to a very good degree.

Having determined the values of apparent activation energies and the conversion functions for crystallization steps 1 and 2, the experimental data were reconstructed numerically by applying the "master plot" method [20]. According to this method, for a single-step process, the following equation is easily derived from Eq. (2), using a reference point at $\alpha = 0.5$:

$$\frac{d\alpha/dt}{(d\alpha/dt)_{\alpha=0.5}} \frac{\exp(E_a/RT)}{\exp(E_a/RT_{0.5})} = \frac{f(\alpha)}{f(0.5)} \tag{9}$$

where $f(0.5)$ is constant for the selected conversion function.

Eq. (9) means that, for selected α, the experimentally determined value of the reduced-generalized reaction rate in the form $((d\alpha/dt)/(d\alpha/dt_{\alpha=0.5}))(\exp(E/RT)/\exp(E/RT_{0.5}))$ and theoretically calculated value of $f(\alpha)/f(0.5)$ are equal when the correct conversion function, $f(\alpha)$, is applied. Fig. 6 shows theoretical master plots of $f(\alpha)/f(0.5)$ versus α, using selected $f(\alpha)$ functions listed in Table 2, together with experimental plots $((d\alpha/dt)/(d\alpha/dt_{\alpha=0.5}))(\exp(E/RT)/\exp(E/RT_{0.5}))$ for crystallization steps 1 and 2.

The best agreement of the theoretical master curves with the experimental master curves was achieved using $g(\alpha) = [-\ln(1-\alpha)]^{1/n}$, where $n = 3$. The model is a very good approximation for the parts of the curves corresponding to lower α, while parts of the curves corresponding to higher α show a discrepancy

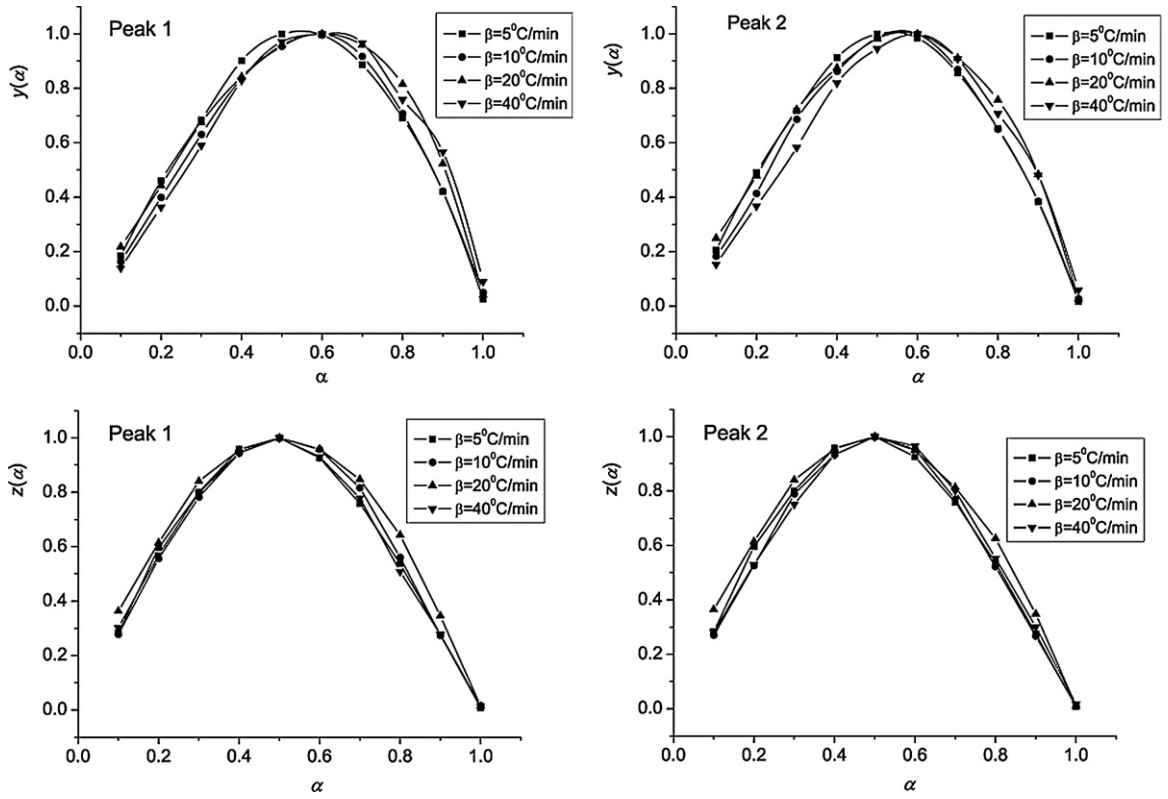

Fig. 5. The normalized functions $y(\alpha)$ and $z(\alpha)$ for peaks 1 and 2.

with the experimental curves. This indicates that, while the model seems to be perfectly valid for the initial part of the reaction, the conditions of the reaction change half-way in such a way that the JMA model is no longer a good description.

3.3. Correlation of established kinetic triplets and structural transformations

Considering the results presented above, we investigated the possible reasons for the deviation of the experimental curves from the theoretical model in the second part of the reaction in detailed correlation of the structural transformations with the conditions inherent in the application of JMA model. The system fits the model well in the first half of the reaction, indicating that primary nucleation is completed before the start of the crystal growth. If nucleation is the cause of this deviation from JMA model, then it must be secondary nucleation, starting at the point in the reaction where the system begins to deviate from the model. This secondary nucleation would proceed in parallel with crystal growth, invalidating the necessary condition for successful application of JMA model. The validity of the JMA equation can be extended to non-isothermal conditions if the entire nucleation process takes place during the early stages of the transformation and becomes negligible afterwards [26,27].

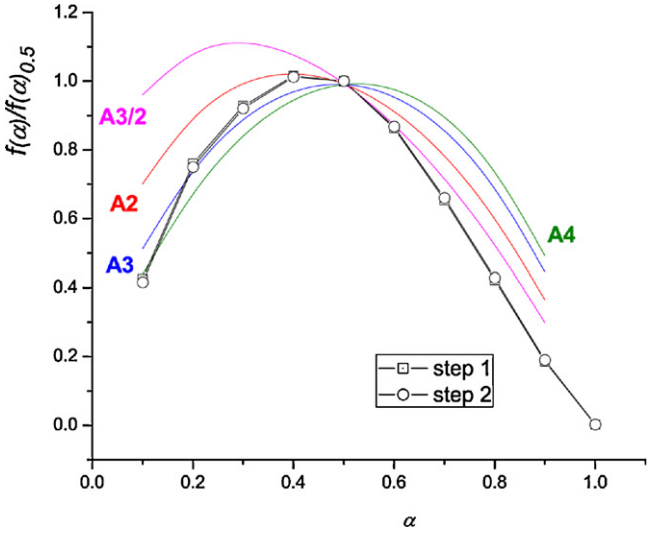

Fig. 6. Theoretical (lines) and calculated (symbols) master curves in differential form representing $f(\alpha)/f(0.5)$ as a function of α for different JMA conversion functions labeled An (n = 3/2 to 4).

According to our results [10], the first two peaks in DSC correspond to the formation of stable crystal phases α-Fe(Si) and Fe_2B, while the third could be attributed to recrystallization of these phases and further growth of crystallites. Using this data, we can elucidate the following sequence of crystallization: first to crystallize is α-Fe(Si) phase, followed by $B_2Fe_{15}Si_3$ and Fe_2B phase. In addition, metastable $B_2Fe_{15}Si_3$ phase subsequently decomposes to yield the two stable crystalline phases, α-Fe(Si) and Fe_2B.

The first peak in the DSC curve would correspond to formation of crystalline α-Fe(Si) in the amorphous matrix, since it is the first to be observed in the XRD spectra (after heating at 723 K). The crystal structure of α-Fe(Si) can accommodate for some of the boron, which destabilizes its lattice and acts as an inhibitor to the crystallization process, causing this reaction to have the highest activation energy and the lowest reaction rate (Table 1). $B_2Fe_{15}Si_3$ stoichiometrically corresponds to $2\times Fe_3B$ plus $3\times Fe_3Si$, and contains only 2.29 mass% of boron, compared to 13% in the as-prepared alloy, but 8.9 mass% of Si, compared to 8% in the as-prepared alloy. All this indicates that $B_2Fe_{15}Si_3$ would probably form around the clusters of short-range crystalline ordering, as those regions probably con-

tain the least amount of amorphizing boron. If this is the case, then its enthalpy of formation would be very low, making it very hard to notice in DSC (Fig. 1).

The second peak in DSC would correspond to crystallization of Fe_2B. This phase contains around 8.8 mass% of boron, compared to 13% in the as-prepared alloy. The formation of this crystalline phase would increase the concentration of boron in the amorphous matrix, making the nucleation of Fe_2B in the amorphous matrix less favorable, meaning that it probably initially occurs through decomposition of the metastable $B_2Fe_{15}Si_3$ phase. The stoichiometry of $B_2Fe_{15}Si_3$ phase indicates that it would probably decompose to Fe_3Si and Fe_3B, where Fe_3B could then easily be converted to Fe_2B by the excess boron in the amorphous matrix. This reaction would have lower activation energy (Table 1), as it would decrease the amount of boron in the surrounding amorphous matrix, and it would create two types of nuclei: one for Fe_2B phase and the other, through Fe_3Si, for α-Fe(Si) phase, providing a source of secondary nucleation for α-Fe(Si).

The third peak in the DSC, which could not be described as a single step process, would correspond to the processes of recrystallization and growth which are observed after the samples have been heated at higher temperatures, as α-Fe(Si) phase gradually gives way to Fe_2B. In this process, Fe_2B nucleates in α-Fe(Si) crystalline matrix, which is probably caused by segregation of boron and Si in α-Fe(Si), where Si-poor regions would allow for nucleation of Fe_2B. This process, as shown by a step-like growth of Fe_2B phase content in XRD spectra, is probably highly dependent on the local composition and lattice structure and the nucleation would happen gradually as favorable conditions are met in any particular area of the sample. This would explain the lowest activation energy of the process (Table 2) and its unusual dynamics (Fig. 5), as nucleation and crystal growth would occur continuously and in parallel, rather than separately and consecutively. In addition, this process would provide secondary nucleation sites for further crystallization of Fe_2B phase. The secondary nucleation for both phases would proceed in parallel with the crystal growth that occurs after the primary nucleation and would invalidate the condition for validity of JMA equation in non-isothermal systems. This would explain the good agreement of the experimental curves with theoretical JMA curves in the first part of the reaction and their subsequent divergence, as the latter part would correspond to the region of secondary nucleation (Fig. 6).

4. Conclusions

Amorphous $Fe_{75}Ni_2Si_8B_{13}C_2$ alloy undergoes multi-step structural transformations, after annealing in 790–860 K temperature range, exhibiting two asymmetric overlapping exo-maximums in DSC, which were resolved. With the increase in the heating rate, the positions of these peaks shifted to higher temperatures. The process of phase transformation involves formation of stable iron-silicon (α-Fe(Si)) and iron–boron (Fe_2B) phases, and metastable iron–silicon–boron ($B_2Fe_{15}Si_3$). The primary crystallization starts with formation of α-Fe(Si) phase in the amorphous matrix, followed by metastable $B_2Fe_{15}Si_3$ and the iron–boron (Fe_2B) phase at temperatures above 780 K. The asymmetric peaks were resolved giving three well-formed peaks corresponding to different steps of the phase transformation. The kinetic parameters corresponding to each step were evaluated and kinetic triplets for the first two crystallization steps were determined, yielding the conversion function in the form $g(\alpha) = [-\ln(1-\alpha)]^{1/3}$, $E_a = 375.1 \pm 0.8$ kJ/mol and $\ln A = 56.2 \pm 1.0$ for step 1; $E_a = 341.6 \pm 0.5$ kJ/mol and $\ln A = 49.3 \pm 0.5$ for step 2 of structural transformation of the alloy. This established kinetic model was confirmed by application of independence of activation parameters on the heating rates criterion and master plot method, using the established kinetic triplets. We have established that the divergence between experimental and theoretical JMA curves is the result of secondary nucleation processes for both stable crystalline phases, which occurs in parallel with crystal growth. In addition, the complexity of continuous process of crystal growth and nucleation of Fe_2B phase out of α-Fe(Si) matrix, which corresponds to step 3 of the structural transformation of the alloy, makes it impossible to describe as a single step process and, in consequence, to determine its kinetic triplet.

Acknowledgement

The investigation was partially supported by the Ministry of Science and Environmental Protection of Serbia, under the following Projects 172015, 172035 and 172037.

References

[1] T. Kulik, J. Non-Cryst. Solids 287 (2001) 145.
[2] I.C. Rho, C.S. Yoon, C.K. Kim, T.Y. Byun, K.S. Hong, Mater. Sci. Eng. B 96 (2002) 48.
[3] T. Gloriant, S. Surinah, M.D. Baro, J. Non-Cryst. Solids 333 (2004) 320.
[4] A.A. Soliman, S. Al-Heniti, A. Al-Hajry, M. Al-Assiri, G. Al-Barakati, Thermochim. Acta 413 (2004) 57.
[5] H.F. Li, R.V. Ramanujan, Thin Solid Films 514 (2006) 316.
[6] H.F. Li, R.V. Ramanujan, Mater. Sci. Eng. A 375–377 (2004) 1040.
[7] J. Bednarcik, R. Nicula, M. Stir, E. Bukel, J. Magn. Magn. Mater. 316 (2007) e823.
[8] D.M. Minić, B. Adnadjević, Thermochim. Acta 424 (2008) 41.
[9] D.M. Minić, A. Maričić, B. Adnadjević, J. Alloy Compd. 473 (2009) 363.
[10] D.M. Minić, A. Gavrilović, P. Angerer, D.G. Minić, A. Maričić, J. Alloy Compd. 476 (2009) 705.
[11] R. Rundel, PeakFit: Technical Guide, Jandel Scientific, 1991.
[12] T. Dergez, F. Konczol, N. Farkas, J. Belagyi, D. Lorinczy, J. Therm. Anal. Calorim. 80 (2005) 445.
[13] H.E. Kissinger, Anal. Chem. 29 (1957) 1702.
[14] T.J. Ozawa, J. Therm. Anal. 29 (1970) 301.
[15] J. Flynn, L. Wall, J. Res. Natl. Bur. Stand. Sect. A 70 (1966) 487.
[16] T.J. Ozawa, Bull. Chem. Soc. Jpn. 38 (1965) 1881.
[17] S. Vyazovkin, C.A. Wight, Annu. Rev. Phys. Chem. 48 (1997) 125.
[18] A.W. Coats, J.P. Redfern, Nature 201 (1964) 68.
[19] A.L. Perez-Maqueda, M.J. Criado, J.F. Gotor, J. Malék, J. Phys. Chem. A 106 (2002) 2862.
[20] J.F. Gotor, M.J. Criado, J. Málek, N. Koga, J. Phys. Chem. A 104 (2000) 10777.
[21] J. Málek, Thermochim. Acta 267 (1995) 61.
[22] J. Málek, Thermochim. Acta 200 (1992) 257.
[23] J. Málek, Thermochim. Acta 355 (1-2) (2000) 239.
[24] M. Avrami, J. Chem. Phys. 9 (1941) 177.
[25] W.A. Johnson, R.F. Mehl, Trans. Am. Inst. Min. Metall. Eng. 135 (1939) 135.
[26] D.W. Henderson, J. Therm. Anal. 15 (1979) 325.
[27] D.W. Henderson, J. Non-Cryst. Solids 30 (1979) 301.